NUKLEONIKA 2016;61(4):443–451
doi: 10.1515/nuka-2016-0073

ORIGINAL PAPER

DE GRUYTER
OPEN

Calculation of edge ion temperature and poloidal rotation velocity from carbon III triplet measurements on the COMPASS tokamak

Matěj Tomeš, Vladimír Weinzettl, Tiago Pereira, Martin Imríšek, Jakub Seidl

Abstract. A high-resolution spectroscopic system for the measurements of the CIII triplet at 465 nm was installed at the COMPASS tokamak. The Doppler broadening and shift of the measured spectral lines are used to calculate the edge ion temperature and poloidal plasma rotation. At first, the spectroscopic system based on two-grating spectrometer and the calibration procedure is described. The signal processing including detection and removal of spiky features in the signal caused by hard X-rays based on the difference in the behaviour of Savitzky-Golay and median filters is explained. The detection and position estimation of individual spectral lines based on the continuous wavelet transform is shown. The method of fitting of Gaussians using the orthogonal distance regression and estimation of the error of estimation of the rotation velocity and ion temperature is described. At the end, conclusions about the performance of the spectroscopic system and its shortcomings based on summary of results calculated from 2033 processed spectral lines measured in 61 shots are drawn and the possible enhancements are suggested.

Key words: high-resolution spectroscopy • spectra processing • peak detection • line detection • line fitting • poloidal plasma rotation • ion temperature

M. Tomeš✉, V. Weinzettl, M. Imríšek, J. Seidl
Ústav fyziky plazmatu AV ČR, v.v.i.,
Faculty of Mathematics and Physics,
Charles University in Prague,
Za Slovankou 3, 18200 Praha 8, Czech Republic,
Tel.: +42 077 758 4641,
E-mail: tomes@ipp.cas.cz

T. Pereira
Instituto de Plasmas e Fusao Nuclear,
Lisboa, Portugal

Received: 3 September 2015
Accepted: 11 April 2016

Introduction

Atomic spectroscopy can provide valuable information about fusion plasma. This is possible due to the fact that properties of radiated photons are governed by ion and electron velocity distributions and densities, electromagnetic fields, and ion species present in a plasma. Specifically, it can be used to calculate ion temperature and ion flow along magnetic flux surfaces in tokamaks called plasma rotation. Knowledge of these two quantities and their spatial and temporal evolution is particularly interesting for studies of plasma confinement modes, namely, L-mode (low confinement mode) and H-mode (high confinement mode). A spectroscopic system lent by the Instituto de Plasmas e Fusao Nuclear, Lisboa, Portugal, was installed at the COMPASS tokamak to investigate the stated plasma properties. The system is based on high-resolution measurements of the CIII triplet at 465 nm and calculation of the ion temperature and poloidal plasma rotation from the spectral line shape and position, respectively. Analysis of measured spectra showed that an enhancement is needed to meet requirements for spatial and temporal profiles of calculated ion temperature and plasma rotation. To remove shortcomings of the system, a

better understanding of its properties is required. Steps made to reach this goal are listed in this article. It includes description of basic properties of the COMPASS tokamak and description of the measurement method. The spectroscopic system is described to allow the reader to understand shortcomings and proposed upgrades, which are summarized after the data analysis method is thoroughly explained, and results of ion temperature and plasma poloidal velocity are elaborated.

Measurements of poloidal plasma rotation and edge ion temperature at the COMPASS tokamak

The COMPASS tokamak [1] in Prague has the major radius $R = 0.56$ m and minor radius $a = 20$ cm and is equipped with two neutral beam injection (NBI) heating systems with 0.3 MW of power each. The pulse length is ≤1 s with plasma current of up to 400 kA and toroidal magnetic field of up to $B = 2.1$ T. Additional parameters of the COMPASS tokamak are listed in Table 1. Main plasma facing components are made of graphite, and thus carbon eroded from divertor and limiters because of plasma-wall interaction processes is transported into the plasma and contaminates it. The fractional abundance in deuterium plasma can reach values up to units of percent which results in high intensity of radiation generated by carbon. This makes spectroscopic studies of the CIII triplet at 465 nm a good tool providing information about poloidal plasma rotation u and edge ion temperature T_i. The poloidal cut of the COMPASS vacuum vessel with the region of interest marked with the black dot is shown in Fig. 1. The expected u at the edge is in orders of kilometers per second and the expected T_i is in order of tens of electron-volts. These expectations put requirements on the measurement system to provide a high spectral resolution to allow calculation of u and T_i with reasonable uncertainties. The length of plasma flat top phases in the COMPASS tokamak and also the time scale of the phenomena of interest (e.g., temporal changes in rotation velocity) require the system to provide temporal resolution in orders of units of microseconds.

Table 1. Main parameters of the COMPASS tokamak

COMPASS parameters	
Major radius	0.56 m
Minor radius	0.2 m
Plasma current	<400 kA
Toroidal magnetic	1.15
Electron density	(1–10) × 10^{19} m^{-3}
Electron temperature	<1.5 keV
Pulse length	<1 s
Plasma types	Limited, diverted
NBI heating	2 × 0.3 MW
Vessel material	Inconel
Limiter material	Graphite
Divertor material	Graphite

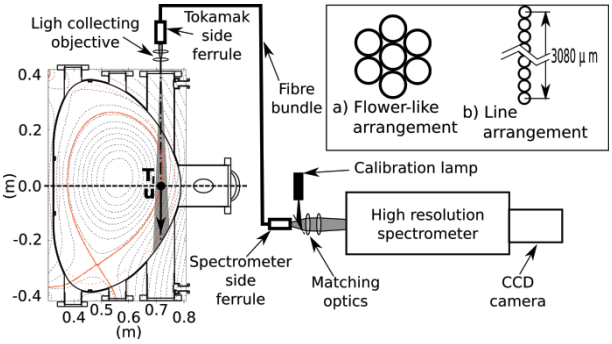

Fig. 1. Left part of the image shows the poloidal cross section of the vacuum vessel with the field of view represented by the yellow cone. The optical path consists of the light collection optics on the tokamak side, fiber bundle, matching optics, spectrometer, and CCD camera. The subfigures (a) and (b) show out of scale schematics of arrangements of fibers in ferrules on the tokamak and spectrometers side, respectively.

CIII triplet and line shape

Calculation of the poloidal plasma rotation velocity and ion temperature are based on the measurements of the carbon III lines at CIII-1 = 464.742 nm, CIII-2 = 465.025, and CIII-3 = 465.147 nm. This is possible because of the fact that the shape and shift of the triplet lines is directly governed by the ion temperature and ion rotation velocity, respectively. All three lines form a triplet with the upper level configuration $p = 1s^2 2s3p$ and the lower level configuration $q = 1s^2 2s3s$. Properties of spectral triplets can be deduced from the spectral emission coefficient of a line, expressed in [2] as

$$\varepsilon_{pq}(\nu,r) = \frac{h\nu_{pq}}{4\pi} A(p \to q) n_i(p,\mathbf{r}) L(\nu,r) \quad (1)$$

The frequency of radiated photon μ_{pq} and the value of Einstein coefficient $A(p \to q)$ are purely functions of atomic properties. The latter is given by the upper and lower levels and the former by their energy difference. The density of upper states $n_i(p,\mathbf{r})$ is a strong function of plasma properties together with $L(\nu,r)$, which is a normalized function describing the line shape. The special properties of spectral multiplets are caused by the fact that the states p and q differ only in angular momentum. As a consequence, all spectral lines in a multiplet are radiated by one population of ions $n_i(p,\mathbf{r})$. This means that the ratio of the lines becomes independent of plasma parameters and the line shape $L(\nu,r)$ is identical. Thus electron temperature cannot be calculated from the ratio of measured carbon III lines. Because line shape $L(\nu,r)$ is a direct function of velocities of radiating ions $n_i(p,\mathbf{r})$, it can be used to calculate the plasma rotation and ion temperature. Ion velocities in plasma in equilibrium can be described by the Maxwell-Boltzmann distribution [3]. The speed distribution along the line of sight (LOS) $\mathbf{v}\cdot\mathbf{LOS}$ can be written as

$$f(r,\nu) = \left(\frac{m_i}{2\pi k_b T(\mathbf{r})}\right) e^{\frac{-m_i(\nu-u(\mathbf{r}))^2}{2k_b T_i(\mathbf{r})}} \quad (2)$$

where m_i is the mass of radiating ion, T_i is the ion temperature, ν is the ion velocity parallel to **LOS**, u is the mean ion velocity (plasma rotation) parallel to **LOS,** and **r** is the position vector. Movement of radiating ions introduces a shift in observed frequency ν of photons described by the Doppler effect [2]

$$\frac{\left(\nu - \nu_u(r)\right) - \nu_{pq}}{\nu_{pq}} = \frac{\nu - u}{c} \tag{3}$$

in terms of radiator's velocity $(\nu - u)$ parallel to **LOS** and frequency ν_{pg} of the photon in the rest frame of the radiator. Solving Eq. (3) for $(\nu - u)$ and plugging the result into Eq. (2) gives the spectral line shape function

$$L(\nu, r) = \sqrt{\frac{mc^2}{2\pi k_b T_i(\mathbf{r})\nu_{pq}^2}}\, e^{\frac{-mc^2\left[\left(\nu-\nu_u(\mathbf{r})\right)-\nu_{pq}\right]^2}{2k_b T_i(\mathbf{r})\nu_{pq}^2}} \tag{4}$$

The term $(\nu - \nu_u(\mathbf{r}))$ is connected to the thermal motion of the radiating ions described in Eq. (2), specifically ν originates from the random ion velocity ν and $\nu_u(\mathbf{r})$ from the mean speed u. This shows that the thermal motion of the radiating ions gives spectral lines a Gaussian shape and can also cause a frequency shift. The width of the line is given directly by the temperature $T_i(\mathbf{r})$ of the ion population $n_i(p,\mathbf{r})$. The mean speed u of the radiating population causes a corresponding spectral shift of the line and can be calculated using the formula for the Doppler shift. A line shape is also influenced by a magnetic field acting on the radiator. This causes changes in the line shape called Zeeman splitting. This effect can be neglected if the formula

$$k_b T_i \geq \frac{1}{2nl}\left(\frac{5a_0^2}{c\mu_0 e}\right)^2 \left(\frac{B\lambda_{pq}}{\frac{a}{a_0}}\right)^2 \frac{m_i}{m_e} E_{\mathrm{H}} \tag{5}$$

given by [4] is fulfilled. Plugging in $l = 1$ for the single electron orbital angular momentum quantum number, $n = 3$ for the principal quantum number, the fine structure constant α, the Bohr radius a_0, the ionization energy of a hydrogen atom E_{H}, and $B =$ 0.89 T for the COMPASS toroidal magnetic field at $R = 0.72$ m gives the result $k_b T_i \geq 8.78$ eV for the CIII triplet. Values of ion temperatures in the region of interest are expected to be above this threshold. The rest of the broadening mechanisms [2, 4], as for example, pressure broadening, are negligible in the COMPASS tokamak plasmas.

Spectroscopic system for CIII triplet measurements

As described in two previous sections, the measurements of CIII triplet at 464 nm with sufficiently high spectral resolution can be used to calculate T_i and u. For this purpose, a spectroscopic system for high temporal and spectral resolution measurements was developed in the Instituto de Plasmas e Fusao Nuclear, Lisboa, Portugal [5, 6], and installed at the COMPASS tokamak. The spectroscopic system consists of five main parts: light collecting objective at the tokamak side, fiber bundle, matching optics at the spectrometer side, high-resolution spectrometer, and charge coupled deviced (CCD) camera. The collecting objective is mounted onto a vertical port, its line of sight is the black dot dashed line in Fig. 1. The objective has demagnification factor of 4 and projects light generated in the field of view showed in Fig. 1 by a yellow cone onto a ferrule of the fiber bundle. The LOS crosses the midplane at approximately $R =$ 0.72 m. The field of view at the midplane covers approximately ±2 cm around the separatrix calculated by EFIT in the flat top phase of a usual discharge. The 4-m long fiber bundle consists of 49 silica fibers with 50 μm core diameter (62.5 μm cladding). The fibers in the tokamak side ferrule are organized as a line of seven flower-like arrangements sketched in Fig. 1a. At the spectrometer side, they are organized as a 3080-μm long single line. The line is projected by the matching optics onto the entrance slit of the spectrometer. The matching optics is equipped with a removable mirror, which switches the optical path to the calibration lamp. This allows the system to be calibrated in the spectral domain. A scheme showing the alignment of the spectrometer, the optical setup at the entrance slit of the spectrometer, and the CCD camera can be seen in Fig. 2. The spectrometer consists of a planar mirror and two spherical gratings with non-equidistant grooving. From the entrance slit, the light incidents onto the first grating named Concave grating 1 in Fig. 2 where it gets dispersed and reflects onto the flat mirror. From the flat mirror, the light is reflected onto the second diffraction grating where it undergoes the second dispersion in the direction of the exit slit and the CCD camera. Owing to the shortness of the fiber bundle, the spectrometer had to be placed in the vicinity of the tokamak. This introduced problems with the interference of the CCD detector with hard X-ray (HXR) radiation generated during a shot. This interference was lowered by lead shielding placed around the spectroscopic camera. The major parameters of the spectroscopic system are listed in Table 2. The recorded spectra were binned (summed) in vertical direction, leaving only the horizontal dimension. In this text, pixel numbering refers to the horizontal rank of the pixel on the CCD chip.

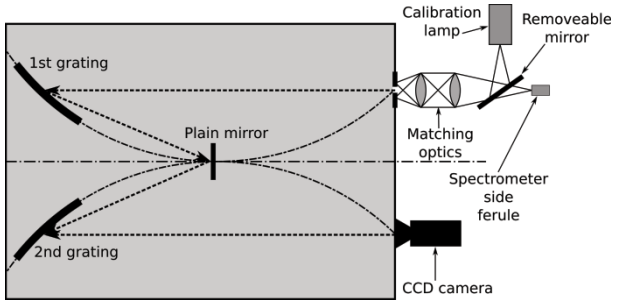

Fig. 2. Scheme showing the alignment of the spectrometer with two spherical gratings and one planar mirror. The matching optics at the entrance slit consists of two lenses and a removable mirror, which allows switching between calibration lamp and the ferrule of the optical fiber.

Table 2. Main parameters of the current spectroscopic system

Temporal resolution	~20 ms
Inverse dispersion	~0.0026 nm/pixel
Spatial imaging	no
Spectrometer numerical aperture (NA)	0.037
Diffraction gratings	2× spherical Non-equidistant 2700 grooves/mm Rectangular (width 6 cm)
Fiber bundle	49 silica fibers 7 spatial points 50 μm diameter NA = 0.22

Spectral calibration of the spectrometer

To allow calculations of plasma properties from measured CIII triplet, spectral calibration and instrumental functions of the spectrometer need to be determined. These were determined from the measurements of spectra of the Fe hollow cathode lamp filled with neon. The calibration function is a mapping from pixels to corresponding wavelengths. In the case of the spectrometer, the linear function showed as an acceptable choice giving sufficiently low errors:

$$f(\lambda) = a \cdot \text{pixel} + b \tag{6}$$

where a is the spectral resolution of the spectrometer. The instrumental function describes broadening of spectral lines by the spectrometer. This can be determined from the width of the lines in calibration spectra. An example of such measured spectra is plotted in Fig. 3 with crosses. It shows 10 visible lines from which only five of them were used for calibration purposes. The unused five lines could not be either properly identified and resolved or are not a single spectral line. The wavelengths λ_{pq} were taken from tables accessible at [7]. To get a better precision of the calibration, the identified lines need to be fitted by an analytical function well approximating the line shape. In this case a Gaussian approximation showed as reasonable. This is supported by a good

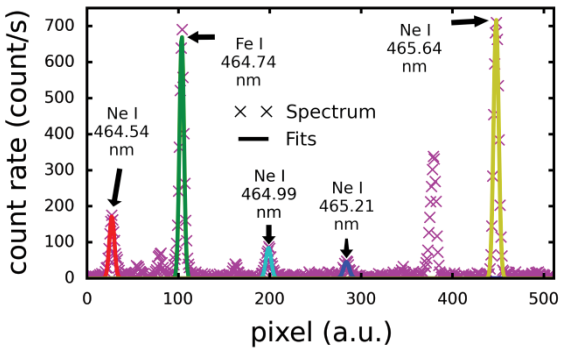

Fig. 3. Processed calibration spectrum. The spectrum is plotted with crosses. The fitted Gaussian-shaped lines are plotted in full line. Unmarked spectral lines are not identified, intensive enough or are multiple unresolved lines.

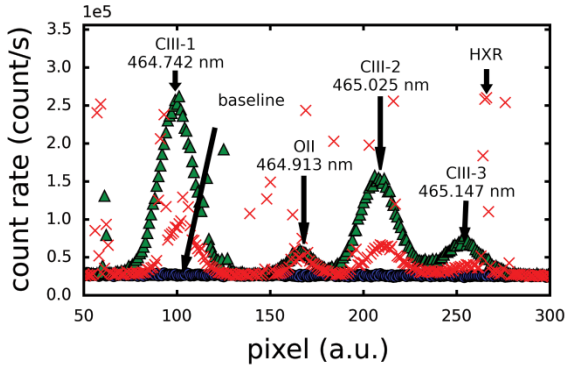

Fig. 4. Spectra measured during shot #6080 with visible CIII triplet and O II lines, HXR interference, and baseline.

agreement of the spectral lines with fits plotted by full lines in Fig. 3. The fitting algorithm provides mean values μ giving spectral position of each line and standard deviations σ giving the line width in pixels. Using μ and corresponding wavelengths λ_{pq}, the calibration function was fitted using orthogonal distance regression, where the weights were the output errors of the Gaussian fits. The instrumental broadening was calculated as weighted mean of σ. This simple calculation of the instrumental function was possible because contributions of the other broadening mechanisms as temperature broadening are negligible because of low pressure and temperature of the calibration lamp. Analysis of the measured calibration spectra showed that the spectral resolution of the spectrometer was ~0.0026 nm per pixel and the instrumental broadening was ~2.5 pixels.

Processing of measured CIII triplet spectra

A set of spectra measured during the discharge #6080 is displayed in Fig. 4, where several features can be noticed. The first are the carbon triplet lines. The second is the O II line at 464.913 nm. The third is the interfering HXR radiation with its spiky feature and the last is the baseline. Before the lines of the carbon triplet are analysed, the baseline has to be subtracted and the HXR spikes removed. The baseline is the result of a superposition of the stray light inside the spectrometer and the thermal noise of the detector. This gives the baseline a non-linear nature. The baseline was approximated by averaging over spectra with no visible spectral lines, which were recorded before and after each discharge. An example is the flat line in Fig. 4. Typically, more than 35 spectra with integration time in the range 20–30 ms were measured during a single discharge sequence. With this setting, at least 10 measurements of the baseline during each shot were taken. The average baseline smoothed with Savitzky-Golay filter is plotted with full line in Fig. 5. The HXR radiation generated during discharges can be detected by the CCD chip, which results in spiky features visible in Fig. 4. These have to be detected and removed. Removing the HXR spikes showed as the most suitable solution. Application of filtering methods in order to replace spikes would change

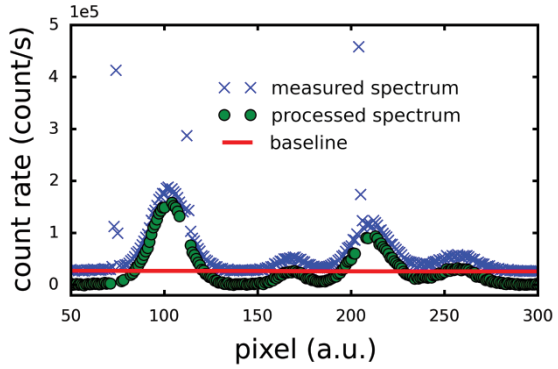

Fig. 5. Measured spectrum #13 in the shot #6080 plotted with crosses, baseline approximation plotted by full line. Spectrum with subtracted baseline and removed HXR interference is plotted with circles.

information in the spectrum (e.g., peak flattening), which is not favourable before further processing including function fitting. Therefore, removal of points containing HXR spikes showed as the most suitable solution. A simple detection algorithm was developed to detect HXR features in a signal. It is based on the difference of behaviour of Savitzky-Golay and median filters. The Savitzky-Golay [8] filtering method is based on polynomial fitting. This can cause the filter to oscillate under a certain circumstances. One of them is a sharp feature in a signal as the HXR spike. A part of a spectrum filtered by a Savitzky-Golay filter is plotted by dashed line in Fig. 6. Oscillation in the filtered signal caused by the HXR spikes can be clearly seen near the pixel 112. It can also be seen that the amplitude of the filtered signal at the position of the HXR spike is lower than the original signal. The spectrum filtered by a median filter is plotted in the same figure by the solid curve. The median filter tends to flatten parts of a spectrum containing spikes. The amplitude of the signal filtered by a median filter at the position of the HXR spike is the lowest of all three signals. Using the described difference in behaviour showed as a suitable base for building an automatic detection of the HXR interference. A spike is recognized when mutual amplitude differences between all three signals (i.e., between original and Savitzky-Golay filtered signals, between original and median filtered signals, and between Savitzky-Golay and median filtered signals) reach a certain threshold. Although this method is not absolutely robust and minor changes based on the shape of the spectrum have to be made occasionally, it showed as a good tool for the detection of the peak in flat parts as well as in parts of spectra containing spectral lines. An example of processed spectrum with subtracted baseline and removed HXR interference spikes is curve in Fig. 5 plotted with circles. As described in section "CIII triplet and line shape", plasma rotation velocity can be calculated from position of a spectral line and the ion temperature from the line width. Both properties can be obtained with a good precision by fitting a Gaussian shape through the spectral lines of the carbon triplet. As it is visible in Fig. 4, two to four spectral lines are usually observable in the measured spectra. Three of them belong to the CIII triplet and are of interest. To provide good initial conditions for fitting routines to converge to a reasonable solution, number of visible spectral lines has to be identified and their position estimated. For this purpose, an algorithm for peak detection based on a filtering of spectra by bank of filters inspired by the continuous wavelet transform (CWT) was developed. The algorithm was inspired by [9]. The discrete wavelet transform [10] can be written in a convolution form:

$$t[n,s] = \sum_{m=0}^{M} f[m]\psi_s(m-n) \tag{7}$$

resembling a filtering of a discrete signal f[m] by a filter ψ_s. A bank of filters ψ_s was constructed using the Hermitian wavelets of the first order

$$\psi_s(n) = \frac{n}{s^3\sqrt{2\pi}} e^{\frac{-n^2}{2s^2}} \tag{8}$$

with scaling coefficient s from 35 to 1. An example of a spectrum filtered by the Hermitian filter with scale $s = 10$ is the solid curve with diamond markers plotted in Fig. 7. Lines and their positions are identified in several steps. In the first step, all zero crossings with the neighbouring local extremes

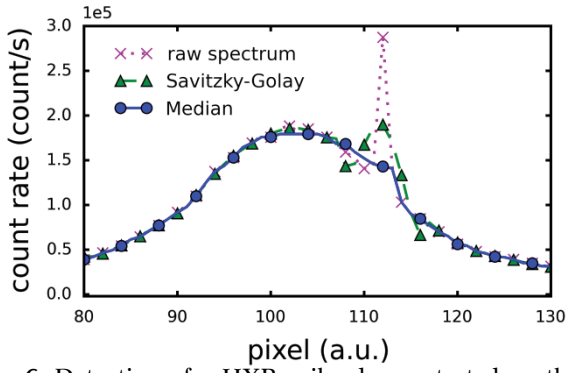

Fig. 6. Detection of a HXR spike demonstrated on the CIII-1 spectral line measured during shot #6080. Raw spectrum (crosses) and spectrum filtered by median (circles) and Savitzky-Golay (triangles) filters are displayed. The difference of all three signals increases in the vicinity of the HXR spike. The detection algorithm is based on this behaviour.

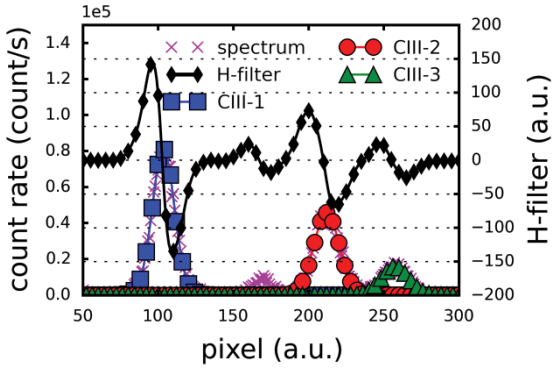

Fig. 7. Processed spectrum measured during shot #6060 (crosses) with plotted Gaussian fits of the individual spectral lines CIII-1, CIII-2, and CIII-3 are marked, respectively, with squares, circles, and triangles. The processed spectrum filtered by the Hermitian filter with scale $s = 10$ (H-filter in the plot) indicates the positions of the spectral lines by signal crossing from positive to negative values.

exceeding a certain threshold are found. In the second step, lines are identified as all such crossings found in the signal filtered by filter with the highest *s*. The line position is then refined by searching for the closest zero crossing in the signal filtered by filter with the second highest *s*. This algorithm is repeated until the lowest *s* is reached. The need for such iteration is given by the presence of noise in the measured spectra. The filter with the highest scaling coefficient is the least vulnerable toward false line detection because of noise but the precision of the line position estimation is the lowest. The filter with the highest *s* serves for the detection of number of visible lines; the lower *s* filters are used for the determination of the position of the detected lines. Once the spectral lines are identified, the upper half of each line is fitted separately by a Gaussian function. An example of a spectrum with four detected lines and over-plotted corresponding Gaussian fits is in Fig. 7. The output of the fitting algorithm is the mean value of the Gaussian that corresponds to the line position λ_D and the standard deviation λ_{fit} that corresponds to the broadening of the line and line intensity. The approach of fitting each line separately and using only the upper halves of the spectral lines showed as robust in the case of partly overlapping lines and toward spectral features caused by spectrometer misalignment.

Calculation of rotation velocity and ion temperature

As described in section "CIII triplet and line shape", knowledge of the line position and width can be used to calculate the rotation velocity and ion temperature, respectively. The rotation velocity u was calculated as

$$u = c\frac{\lambda_D - \lambda_{pq}}{\lambda_{pq}} \tag{9}$$

The ion temperature was calculated using the full width half maximum of the line fit $\Delta_{fit} = 2\sqrt{\ln 2}\sigma_{fit}$ and

$$kT_i = \frac{m_i c^2}{8e\cdot\ln 2}\frac{\Delta_{fit}^2 - \Delta_{inst}^2}{\lambda_{pq}^2}[\mathrm{eV}] \tag{10}$$

in the frame of Δ_{inst} being the instrumental width of the spectrometer calculated from calibration measurements and m_i being the mass of carbon III ion. The value of velocity uncertainty σ_u was calculated using

$$\sigma_u = \sqrt{\left(c\frac{1}{\lambda_{pq}}\sigma_{\lambda_D}\right)^2 + \left(c\frac{-\lambda_D}{\lambda_{pq}^2}\sigma_{\lambda_{pq}}\right)^2} \tag{11}$$

where $\sigma_{\lambda_{pq}}$ is the uncertainty of the radiated wavelength in the rest frame of the ion obtained from [7]. The uncertainty of the fitted line position σ_{λ_D} consists of the contribution from the error of the calibration and the error of the fit supplied by the fitting routine. The uncertainty of ion temperature calculation is given by

$$\sigma_{kT_i} = \frac{m_i c}{8e\cdot\ln 2}\sqrt{\left(\frac{2\Delta_{fit}}{\lambda_{pq}^2}\sigma_{\Delta_{fit}}\right)^2 + \left(\frac{2\Delta_{inst}}{\lambda_{pq}^2}\sigma_{\Delta_{inst}}\right)^2 + \left(\frac{2\left(\Delta_{fit}^2 - \Delta_{inst}^2\right)}{\lambda_{pq}^3}\cdot\sigma_{\lambda_{pq}}\right)^2} \tag{12}$$

where the σ_Δ is the contribution of the error of the Gaussian fit of the line and the error of the calibration. The instrumental width Δ_{inst} is obtained from the calibration together with the uncertainty $\sigma_{\Delta_{inst}}$. Both σ_u and σ_{kT_i} were calculated using the standard formula for uncertainty propagation. They are based only on contributions which can be calculated during the data processing and calibration and do not take into account uncertainty contributions of instruments of the spectroscopic system.

Calculated edge ion temperatures and poloidal rotation velocities

Results presented in this paper were measured during 61 shots during which 716 spectra were measured and 2033 spectral lines were detected. For calibration purposes, a set of nine calibration spectra were measured. Spectra measured during discharges were sorted into groups by the temporal separation from the calibration measurements. Analysis showed that the average reached spectral resolution is ~0.0026 nm per pixel. Without fitting of line shapes, this gives for a noiseless signal uncertainty ~800 m·s^{-1} in velocity and ~2.0 eV in temperature. Probability mass functions of uncertainties of calculated T_i and u for all analysed spectra are displayed in Figs. 8 and 9. Comparison of estimated and reached values of uncertainties shows that the used fitting procedure can on an average improve the precision by factor of two in the case of calculation of poloidal rotation velocity and by factor of four in the case of calculation of ion temperature. An example of a time evolution of u and T_i calculated for shot #6056 is displayed in Figs. 10 and 11. Square, circle, and

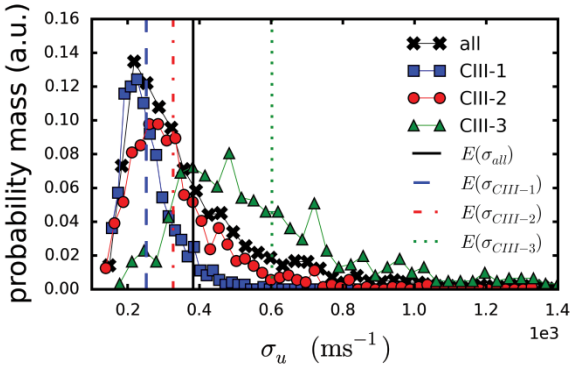

Fig. 8. Probability mass functions of uncertainties for ion rotation velocities calculated from individual spectral lines and averaged over all spectral lines. The vertical lines show mean uncertainty of calculated ion rotation velocities: $E(\sigma_{all})$ = 390 m·s^{-1}, $E(\sigma_{CIII\text{-}1})$ = 260 m·s^{-1}, $E(\sigma_{CIII\text{-}2})$ = 330 m·s^{-1}, and $E(\sigma_{CIII\text{-}3})$ = 610 m·s^{-1}.

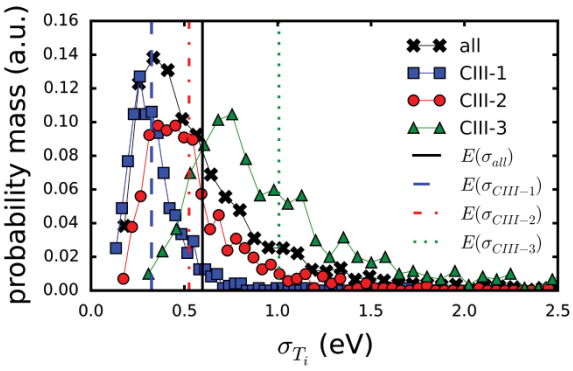

Fig. 9. Probability mass functions of uncertainties of ion temperatures calculated from individual spectral lines and averaged over all spectral lines. The vertical lines show mean uncertainty of calculated ion temperatures: $E(\sigma_{all}) = 0.6$ eV, $E(\sigma_{CIII\text{-}1}) = 0.3$ eV, $E(\sigma_{CIII\text{-}2}) = 0.5$ eV, and $E(\sigma_{CIII\text{-}3}) = 1.0$ eV.

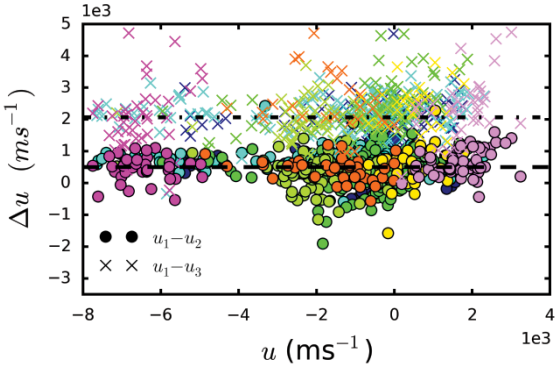

Fig. 12. Differences in rotation velocity calculated from individual spectral lines for spectra measured in a number of shots. The dashed and dot-dashed lines correspond to the mean values of all displayed $u_1 - u_2$ and $u_1 - u_3$, respectively. The colours group data calculated from individual shots.

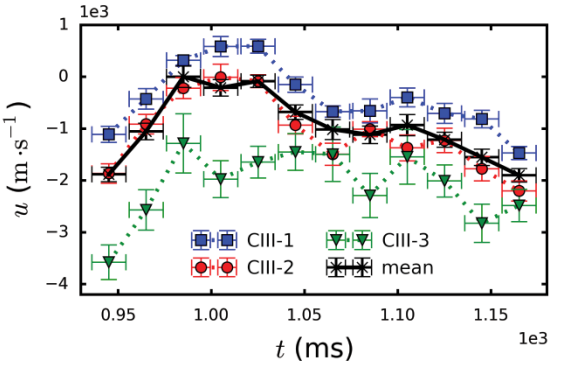

Fig. 10. Calculated temporal evolution of poloidal rotation velocity for the shot #6056. Values plotted with square, circle, and triangle markers are calculated from the spectral lines CIII-1, CIII-2, and CIII-3, respectively. Trace plotted with crosses and full line is calculated as a weighted mean of the three latter values.

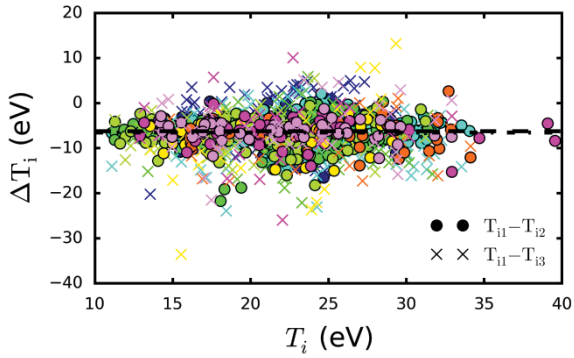

Fig. 13. Differences in ion temperature calculated from individual spectral lines for spectra measured in a number of shots. The overlapping dashed and dot-dashed lines correspond to the mean values of all displayed $T_{i1} - T_{i2}$ and $T_{i1} - T_{i3}$, respectively. The colours group data calculated from individual shots.

triangle markers show, respectively, values calculated from CIII-1, CIII-2, and CIII-3 spectral lines. Values plotted with crosses are weighted mean averages where the contributors are the values calculated from the individual spectral lines and the weights are inverse values of their uncertainties. A clear separation between the curves is noticeable in both Figs. 8 and

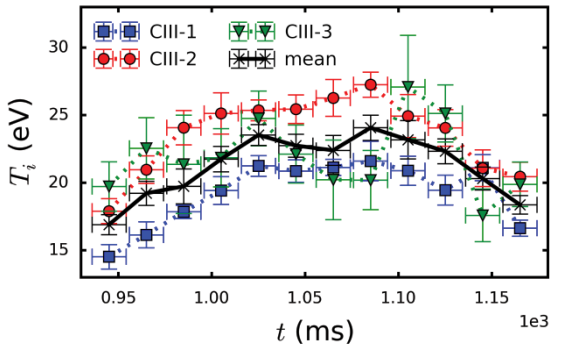

Fig. 11. Calculated temporal evolution of edge ion temperature for the shot #6056. Values plotted with square, circle, and triangle markers are calculated from the spectral lines CIII-1, CIII-2, and CIII-3, respectively. Trace plotted with crosses and full line is calculated as a weighted mean of the three latter values.

9, although calculation from all three spectral lines should yield the same results as described in section "CIII triplet and line shape". This bias is present in the whole set of processed data. Differences in results $u_1 - u_2$, $u_3 - u_1$, $T_{i1} - T_{i2}$, $T_{i1} - T_{i3}$ plotted in Figs. 12 and 13 show that results are shifted by $E(u_1 - u_2) = 500$ m·s^{-1}, $E(u_1 - u_3) = 2070$ m·s^{-1}, $E(T_{i1} - T_{i2}) = -6.2$ eV, $E(T_{i1} - T_{i3}) = -6.5$ eV. Another important property is the independence of the error on the group of measurements. The strong bias suggests a systematic error in the measuring technique or data analysis, otherwise the mean values would be close to zero. The independence on the calibration procedure suggests that the systematic error is probably caused by the measurement technique.

Conclusions

The goal of the measurements of the CIII triplet is to collect information about both edge plasma poloidal rotation and ion temperature. The temporal and spatial resolution should allow observation of time-space evolution of both quantities in proximity of separatrix and study of the influence of plasma parameters and confinement modes. To evaluate the

properties of the spectroscopic system, a representative set of data was measured and a thorough method of data analysis was developed. The requirements on the spectral resolution were given by expected values of edge plasma poloidal rotation and ion temperature, which were estimated in units of km·s^{-1} and tens of eV, respectively. The developed calibration procedure allowed to estimate the typically reached spectral resolution as 0.0026 nm per pixel, which corresponds to the uncertainty in plasma rotation velocity of ∼800 m·s^{-1} and ∼2 eV in temperature. The measured instrumental broadening of a spectral line is $\Delta_{inst} = 0.017$ nm. Examination of the measured spectra of the CIII triplet showed that two unwanted signal features have to be carefully removed before the data processing. The first feature is the baseline, which is most likely a superposition of the detector noise and the stray light inside the spectrometer. The second feature is interference of the HXR radiation generated during a discharge with the CCD chip. A procedure for the detection and removal of both features was developed and tested on the set of measured data. Although not completely automatic, the developed algorithms showed as robust towards noise and wide magnitude of spectral line intensities. Preprocessed spectra were then analysed by an algorithm designed for automatic detection and fitting of the spectral lines. The lines were detected using a bank of filter based on CWT and Hermitian wavelets. The fitting routine used orthogonal distance regression which allows to take into account errors in both dependent and independent variables. This was used to estimate uncertainties of the calculated edge poloidal rotation velocity and ion temperature. Both developed algorithms were applied on 716 spectra measured in 61 shots in which 2033 spectral peaks were detected and analysed. Calculated poloidal rotation velocities were in the range from –10 to 2 km·s^{-1} with average uncertainty $\sigma_u = 380$ m·s^{-1}. The average uncertainty is lowered by Gaussian fitting, which allows to determine the line position with subpixel precision. The ion temperatures were in the range from 10 to 50 eV with mean uncertainties of 0.6 eV. The bottom level is at the edge of the threshold given by the Zeeman broadening specified in Eq. (5). Comparison of u and T_i showed a nonzero mean shift of results calculated from different spectral lines. This suggests a systematic error of the measurement method. The shift showed to be dependent on the wavelength (spectral line) and independent of the wavelength shift, line broadening, line intensity, or calibration measurement. The probable source of this error is difference in position of the focus of the light from the fiber bundle and Fe calibration lamp. The position of the focus influences the position of spectrum on the detector. This would cause a shift in wavelength axis between the calibration and CIII triplet measurements. This shift then causes the systematic error in calculated u and T_i visible on a comparison of the results from individual spectral lines. The careful analysis of the data showed that the calibration procedure has to be changed to remove the described systematic error, the spectrometer should be moved from the tokamak hall to reduce the HXR interference, the throughput of the system has to be increased to allow a better temporal resolution and a new configuration of the spectrometer allowing spatial imaging has to be found. A new fiber bundle with 32 + 2 fibers with diameter of 200 μm and numerical aperture (NA) of 0.22 has been recently purchased. Two of the fibers in the spectrometer ferrule are not included in the bundle and are terminated with separate SMA connectors. This solution will allow the two fibers to collect the light from the calibration lamp even during the measurements of the CIII triplet while keeping the same focus point. The installation of the new fiber bundle will not only remove the systematic error but also increase the number of possible spatial points to 32. The length of the fiber bundle will also allow movement of the spectrometer outside of the tokamak hall, which should largely reduce the interference of HXR with the CCD chip. To allow spatially resolved measurements, a new alignment of the spectrometer had to be calculated. Imaging properties of the spectrometer were reached, but further work has to be made to verify the influence of the new alignment on the spectral resolution and NA of the spectrometer. NA of the new alignment should match better the NA of the new fiber bundle. This will increase the throughput of the spectroscopic system and allow a better temporal resolution. More work is being done to fully investigate properties of the new system.

Acknowledgments. This project has received funding from the European Union's Horizon 2020 Research and Innovation programme under grant agreement no. 633053. The views and opinions expressed herein do not necessarily reflect those of the European Commission. Gratitude is also extended to the project MSMT #8D15001 for the received support.

References

1. Panek, R., Bilková, O., Fuchs, V., Hron, M., Chraska, P., Stockel, J., Urban, J., Weinzettl, V., Zajac, J., & Zacek, F. (2006). Reinstallation of the COMPASS-D tokamak in IPP ASCR. *Czech. J. Phys., 56*(Suppl.2), B125–B137. DOI: 10.1007/s10582-006-0188-1.
2. Kunze, H. J. (2009). *Introduction to plasma spectroscopy*. Berlin-Heidelberg: Springer.
3. Boyd, T. M. J., & Sanderson, J. J. (2003). *The physics of plasmas.* New York: Cambridge University Press.
4. Griem, H. R. (1997). *Principles of plasma spectroscopy*. Cambridge, UK: Cambridge University Press.
5. Gomes, R. B., Varandas, C. A. F., Cabral, J. A. C., Sokolova, E., & Cortes, S. R. (2003). High dispersion spectrometer for time resolved Doppler measurements of impurity lines emitted during ISTTOK tokamak discharges. *Rev. Sci. Instrum., 74*(3), 2071–2074. DOI: 10.1063/1.1537039.
6. Sokolova, E., Cortes, S. D. R., & Nelson, M. (1997). High-resolution spectrometer for TOKAMAK plasma diagnostic. *SPIE*, *3130*, 160–167. DOI: 10.1117/12.284058.
7. Kramida, A., Ralchenko, Yu., Reader, J., & NIST ASD Team. (2014). *NIST Atomic Spectra Database (ver.*

5.2). Retrieved July 27, 2015, from http://physics.nist.gov/asd
8. Savitykz, A., & Golay, M. J. E. (1964). Smoothing and differentiation of data by simplified least squares procedures. *Anal. Chem., 36*(8), 1627–1639. DOI: 10.1021/ac60214a047.
9. National Instruments. (2013, August). *Wavelet-based peak detection*. Retrieved March 10, 2015, from http://www.ni.com/white-paper/5432/en/
10. Mallat, S. (2009). *A wavelet tour of signal processing: the sparse way* (3rd ed.). Boston: Elsevier/Academic Press.